Presented at the IEEE Nuclear
Science Symposium Semiconductor
Short Course, October 21-23, 1981
San Francisco, California.
To be published in the IEEE
Transactions on Nuclear Science,
June 1982

LBL-14145

LBL--14145

DE82 013003

FAST-TIMING METHODS FOR SEMICONDUCTOR DETECTORS

Helmuth Spieler

GSI - Gesellschaft fuer Schwerionenforschung
6100 Darmstadt, West Germany

and

Lawrence Berkeley Laboratory
University of California
Berkeley, California 94720 U.S.A.

March, 1982

Prepared for the U. S. Department of Energy
under Contract DE-AC03-76SF00098

LBL-14145

FAST TIMING METHODS FOR SEMICONDUCTOR DETECTORS

Helmuth Spieler

GSI - Gesellschaft fuer Schwerionenforschung
6100 Darmstadt, West Germany

and

Lawrence Berkeley Laboratory*
University of California
Berkeley, California 94720 U.S.A.

ABSTRACT

This tutorial paper discusses the basic parameters which determine the accuracy of timing measurements and their effect in a practical application, specifically timing with thin-surface barrier detectors. The discussion focusses on properties of the detector, low-noise amplifiers, trigger circuits and time converters. New material presented in this paper includes bipolar transistor input stages with noise performance superior to currently available FETs, "noiseless" input terminations in sub-nanosecond preamplifiers and methods using transmission lines to couple the detector to remotely mounted preamplifiers. Trigger circuits are characterized in terms of effective rise time, equivalent input noise and residual jitter.

1. INTRODUCTION

Fast timing with semiconductor detectors is a many-faceted subject, where the multitude of relevant details can easily obscure the fact that the performance of all timing systems is determined by only a few basic principles. The purpose of this tutorial paper is to point out these principles and demonstrate how they apply to a specific situation. For clarity this demonstration will be restricted to thin surface barrier detectors. This choice is justified by the fact that systems using these detectors not only provide the best time resolution currently being obtained with semiconductor detectors, but that they also have the potential for significant improvement.

A typical nuclear detector system using surface barrier detectors is the ΔE-E time-of-flight telescope. Figure 1 shows the basic configuration of such a system: a thin transmission detector (ΔE) and a stop detector (E) are spaced so that particles passing through the start detector traverse a distance s before impinging on the stop detector. The time-of-flight t between the two detectors is measured, which, together with the energy E measured in the stop detector, permits calculation of the particle mass:

$$m = \frac{2}{s^2} \cdot E\, t^2 \qquad (1)$$

Experimental results[1] for a typical system are shown in Fig. 2. In this measurement the thickness of the ΔE detector was 24 μm, that of the E detector 58 μm. Mass resolution of 0.4 amu was obtained by a 19 cm flight path and an overall time resolution of 85 ps FWHM. The relationship between ΔE and E yields the atomic number Z of the reaction products as shown in the Z-spectrum (Fig. 2b). Event by event sorting of m according to bins in the Z-spectrum, corresponding to individual atomic numbers A, yields unambiguous identification of the reaction channels (more than 20

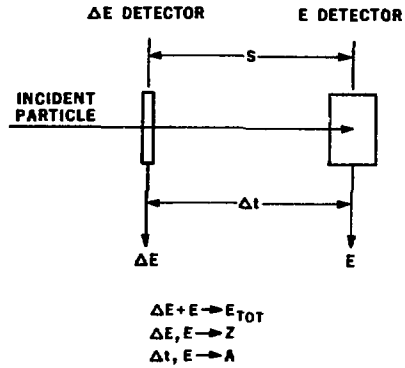

XBL 822-8106

Fig. 1. Configuration of a ΔE-E Time-of-Flight (TOF) Telescope.

in the example shown). Gating m with Z = 8, for example, results in the mass spectrum of oxygen isotopes (Fig. 2c).

Time resolution of 50 to 100 ps is being obtained routinely by several experimental groups.[2-4] In order to recognize and understand the limiting factors in these measurements it is necessary to systematically evaluate the contributions of all components in the timing system.

2. SYSTEM COMPONENTS AND BASIC CRITERIA

The basic semiconductor detector timing channel is shown in Fig. 3. Its components are:

1. A detector, which produces a current or voltage pulse when a particle deposits energy in its sensitive volume.

2. A series of amplifiers, which present the appropriate impedance to the detector and amplify the detector signal by an amount sufficient to drive the trigger circuit.

3. A trigger (often called a discriminator), which furnishes a normalized logic pulse with a well defined time relationship to the (variable) input signal and ultimately to the physical cause of this signal, i.e. the particle impinging on the detector.

*Present Address

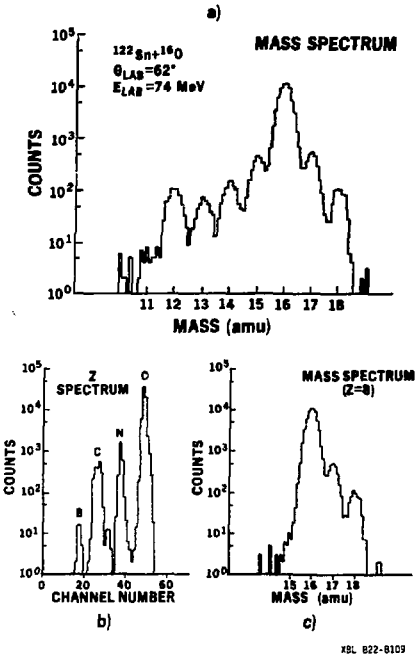

Fig. 2. Total mass spectrum (a), Z-spectrum (b) and mass spectrum for Z = 8 (c) taken with a ΔE-E TOF telescope.

4. A time digitizer, which measures the time difference between the detector signal and a reference channel, either a second detector - as in the TOF telescope - or a fast buncher determining the time structure of a pulsed accelerator beam.[5-7] Typically this is a combination of a time-to-amplitude converter (TAC) and an ADC.

Before investigating these individual components in detail, we must establish the basic criteria which determine time resolution.

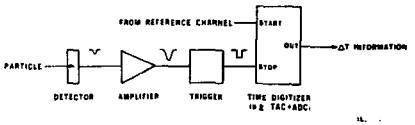

Fig. 3. Basic components of a timing channel.

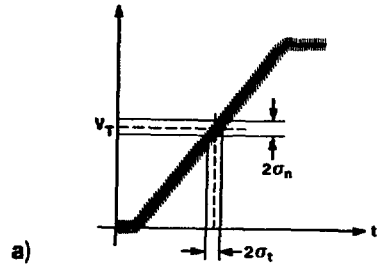

$$\sigma_t = \frac{\sigma_n}{\left(\frac{dV}{dt}\right)_{V_T}}$$

$$\Delta t = 2.35 \cdot \frac{\sigma_n}{\left(\frac{dV}{dt}\right)_{V_T}}$$

OPTIMUM TRIGGER LEVEL:

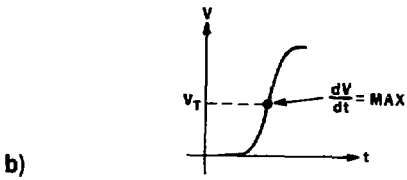

XBL 822-8095

Fig. 4. Parameters which determine time resolution.

If a noisy analog pulse is applied to a leading edge trigger, (i.e., a circuit producing a logic pulse *when the input signal exceeds* a fixed threshold level) the timing uncertainty can be obtained by a simple geometric transformation (Fig. 4a). Projecting the variance σ_n of the momentary signal amplitude on its rate of change dV/dt at the trigger threshold V_T yields the variance in time σ_t of the output pulse, called "jitter".

$$\sigma_t = \frac{\sigma_n}{\left(\frac{dV}{dt}\right)_{V_T}} \qquad (2)$$

in general

$$\sigma_t = \frac{\sigma_n}{\left(\frac{dV}{dt}\right)_{V_T}} + \delta t \qquad (3)$$

where δ_t represents transit time differences in the detector or associated electronics (residual jitter). σ_n represents amplitude variations of any kind, not only noise but also variations in pulse shape. If σ_n is determined by noise alone it is equal to the rms noise voltage. Multiplying the standard deviation σ_t by 2.35 yields the time resolution FWHM. Minimum jitter results when the trigger threshold is set at the point of maximum slope dV/dt of the pulse transition (Fig. 4b).

Qualitatively, this relationship shows that increasing signal-to-noise ratio, decreasing rise time and decreasing residual jitter lead to improved time resolution. Furthermore, if σ_n and $(dV/dt)_{V_T}$ are accurately measured, this equation provides a quantitative benchmark against which the characteristics of a detector (st) or the electronics can be measured. This is one of the most important tools in estimating the capabilities of a timing system and its individual components.

3. THE DETECTOR

Electron-hole pairs are formed along the track of the incident particle in proportion to the stopping power of the detector material. The electrons and holes are accelerated toward the positive and negative electrode respectively, attaining a velocity of

$$\vec{v}(x) = \mu \cdot \vec{E}(x) \qquad (4)$$

where $\vec{E}$ is the local electric field strength and μ is the mobility of the charge carriers. The mobility of electrons μ_- is roughly three times as large as the mobility of holes μ_+. Carrier mobility is constant at low fields $E < E_c$, where $E_c \approx 2.5 \cdot 10^3$ V cm^{-1} for electrons and $E_c \approx 7.5 \cdot 10^3$ V cm^{-1} for holes in silicon at room temperature.[8] Under these conditions $\mu_- \approx 1350$ cm^2 V^{-1} s^{-1} and $\mu_+ \approx 480$ cm^2 V^{-1} s^{-1}. At high fields ($E > 5 \cdot 10^4$ V cm^{-1}) carrier mobility becomes inversely proportional to the electric field so that the charge carriers attain a saturation velocity independent of field strength, corresponding to a transit time of 10 ps per μm detector thickness.

Application of a reverse bias voltage V_b to a surface barrier or junction detector results in a depletion region of thickness

$$d = \sqrt{2 \varepsilon \mu_- \rho V_b} \qquad (5)$$

where μ is the mobility of the majority carriers, ρ the resistivity and ε the dielectric constant of the semiconductor material. If d is smaller than the thickness D of the semiconductor wafer (partial depletion) the electric field distribution is

$$E(x) = \frac{d-x}{\mu \rho \varepsilon} \qquad (6)$$

(Fig. 5a). The maximum field strength at the junction ($x = 0$) is

$$E_{max} = \sqrt{\frac{2V_b}{\mu \rho \varepsilon}} = \frac{2V_b}{d} \qquad (7)$$

The depletion depth and the maximum field strength both increase with the square root of the applied bias voltage. The electric field – and therefore the carrier drift velocity – decreases linearly towards zero at the end of the depletion region, leading to long total collection times.

A more uniform field distribution results from "overbiasing" the detector, that is applying a bias voltage in excess of that required for total depletion of the semiconductor wafer ($d = D$). The minimum field strength in the depletion region then increases to

$$E_{min} = \frac{V_b - V_D}{D}$$

where V_D is the bias voltage required for total depletion. The field strength rises linearly toward the front contact attaining a maximum value

$$E_{max} = E_{min} + \frac{2V_D}{D} \qquad (8)$$

as shown in Fig. 5b. As a practical aid the above relationships expressed in technical units are compiled in the Appendix.

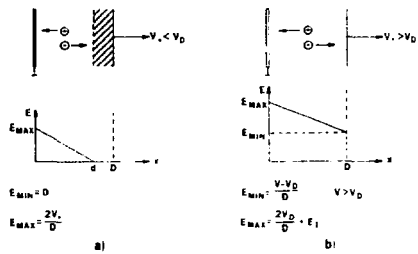

Fig. 5. Electric field distribution in a partially depleted (a) and a totally depleted detector (b).

The motion of a carrier with charge e in the detector volume induces a charge on the detector electrodes at a rate[9]

$$\frac{dq}{dt} = \frac{e v_x}{d} = \frac{e \mu E(x)}{d} \qquad (9)$$

corresponding to the current which would flow into an external circuit with zero impedance. Summing the contributions as a function of time of all charges as they move from their respective positions along the particle track to the corresponding electrodes yields the total current pulse. The induced charge is obtained by integrating the signal current over the collection time, with the interesting result for the incremental induced charge

$$\delta Q = \frac{\delta x}{d} Q \qquad (10)$$

where Q is the total charge produced by the ionizing particle and $\Delta x/d$ is the fraction of the detector thickness which the charge has traversed.[10] A precise calculation of the induced pulse shape must include the variation of ionization density along the particle track, the electric field profile and the velocity dependence of carrier mobility, which is cumbersome but easily done with a computer. However, a quick estimate of the collection time can be made by multiplying the thickness of the detector by the average incremental collection time (e.g., 15 ps/μm for electrons at $(E \approx 2 \cdot 10^4$ V cm^{-1}).

The following general conclusions can be drawn from the preceding discussion:

1. High field strengths are required to reduce collection time, i.e. increase dV/dt.

2. For a given depletion depth, the average field strength will be higher in a detector fabricated from low resistivity material.

3. In order to obtain high field strengths throughout its sensitive volume the detector must be overbiased. The greater the relative overbias V_b/V_D, the more uniform the field profile will be.

4. The collection time in thin detectors is extremely small, as low as 500 ps for 50 μm depletion depth, for example.

Confusion is widespread among experimenters regarding overbias and its effect on collection time. Specifying overbias, i.e. the ratio of applied voltage to depletion voltage by itself, only indicates the ratio of maximum to minimum (non-zero) field strength in the detector. Collection time - the more relevant parameter for timing purposes - is dependent on the magnitude of the electric field, and this is the quantity which should be considered.

Selection criteria for the optimum thickness of the stop detector are not immediately clear. If timing is derived from the current pulse (see Section 4), the thinnest possible detector (thickness equal to particle range) will provide the maximum current as indicated by Eq. 9. On the other hand, if the voltage pulse, i.e. the current pulse integrated on the detector capacitance, is used the signal amplitude V_s is determined by the detector capacitance C_D

$$V_s = \frac{\int i\,dt}{C_D} = \frac{Q}{C_D} \propto Q \cdot D \qquad (11)$$

In this case the signal amplitude will increase with detector thickness (decreasing capacitance). Figure 6 illustrates the situation for two cases: 1) detector thickness equal to particle range ($D = R$), and 2) detector thickness equal to five times particle range ($D = 5R$). Equal field strength, uniform throughout the detector, is assumed in both cases. For $D = R$ the peak amplitude of the current pulse i_s is five times as large as for $D = 5R$. However, for the thicker detector the voltage pulse has five times the amplitude as compared to the thinner detector and despite the larger collection time still has a 20% larger rate of change $(dV/dt)_{max}$. Figure 6b also illustrates that total collection time will be smaller for a thick detector ($D \gg R$) made of n-type, rather than p-type material, since the major part of the pulse is due to the faster carriers. However, as brought out in Fig. 6a, the portion of maximum slope dV/dt rather than the total collection time is relevant for timing applications.

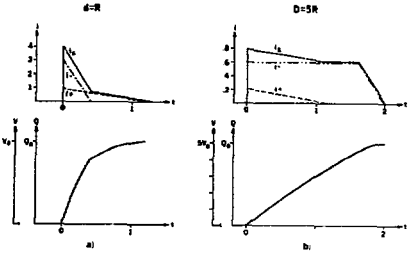

Fig. 6 Current (top) and charge or voltage pulse shapes (bottom) for two detectors: one where the detector thickness equals the range of the incident particle (a), and one where the detector thickness is five times the range (b). i_+ and i_- denote the current pulses due to holes and electrons, respectively. i_s is the total current pulse.

The seemingly obvious advantages of using the current pulse for timing purposes tend to vanish when a practical system is considered. For example, the attainable rise time is limited by the input time constant $C_D \cdot R_i$ of the detector capacitance and the input resistance R_i of the preamplifier. For a given value of R_i the larger capacitance of the thin detector will therefore compensate the advantage of the larger pulse amplitude by increasing the rise time. As will be discussed in Section 4, current mode operation is impractical for thin, high capacitance detectors. Therefore, the following discussion will focus on exploiting the voltage pulse.

The best timing for the voltage pulse is obtained on that portion of the transition where both electrons and holes contribute to maximize dV/dt. Magnitude and slope of this portion remains unchanged when the detector thickness is increased beyond $D \approx 3R$ (the thickness where the collection times for electrons and holes are equal), provided the field strength is maintained at the same value. However, this invariably is the practical limitation when selecting a detector. For use as Δ detectors totally depleted detectors of 50 to 200 μm thickness usually offer the best compromise between high field strength and low capacitance. The thinner detectors usually allow higher field strengths. Another drawback of using too thick a detector arises when the portion of maximum slope is so small, that it cannot be utilized due to the pulse curvature introduced at the pulse origin by multiple integration, which is the rule in fast pulse systems.

High resistivity detectors operated with considerable overbias would provide the most uniform field profile, but commonly available detectors of this type generally cannot withstand the higher field strength, breakdown usually occurring at the "resistive" contact. Detectors made of low resistivity material (ρ = 100 to 1000 Ω cm) require higher depletion voltages to begin with, and with overbias will usually sustain minimum field strengths of $2 \cdot 10^4$ V cm^{-1} or more reliably. Exceptional devices tolerate $5 \cdot 10^4$ V cm^{-1} or more.

In the ΔE transmission detector, range always equals detector thickness, which is selected on the basis of dynamic range in particle identification. For timing considerations the ΔE detector should be chosen as thick as possible, providing a larger signal by virtue of both the increased energy loss and the reduced capacitance.

As a general rule the area of the detector should be chosen as small as can be justified, since the capacitance directly affects the signal-to-noise ratio. Charge collection is usually poor near the periphery of the detector and a suitable aperture should be used to block the outer millimeter or so.

The preceding discussion has emphasized processes in the depletion region in determining pulse shape and timing accuracy. As a next step, it is necesary to consider the effect of the signal path and of imperfections in the detector.

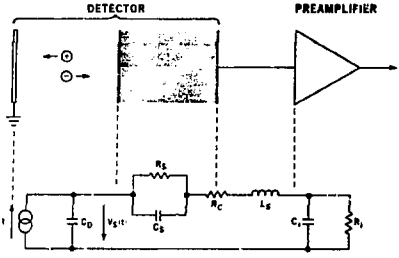

Fig. 7. Equivalent circuit of a partially depleted detector with preamplifier.

Figure 7 shows the equivalent circuit of a partially depleted detector. Charge collection and the depletion region are represented by a signal current source $i_S(t)$ and a shunt capacitance C_D on which the signal voltage $v_S(t)$ is produced. The undepleted bulk silicon between the depleted volume and the resistive contact is equivalent to a parallel RC combination R_S, C_S. The resistance associated with the rear contact is R_C and the inductance of the output connection L_S. The input impedance of the preamplifier exhibits a resistive and a capacitive component R_i and C_i.

The time constant $R_S C_S$ is a material constant independent of bias voltage

$$\tau_S = R_S C_S = \rho\varepsilon \qquad (12)$$

which can be expressed numerically as

$$\tau_S = 1.06 \cdot 10^{-3}\ \rho \qquad (13)$$

where τ_S is expressed in ns and ρ in Ω cm. The equivalent impedance of this circuit is resistive for frequencies $\omega < 1/\tau_S$, a condition which is usually fulfilled in practical situations. A series resistance in the signal path forms an integrator with the preamplifier input capacitance C_i, degrading the obtainable rise time. This series resistance is increased significantly over the DC value since the charge induced on the electrode by the moving column of collected charge is concentrated on a small area, whose order of magnitude corresponds to the lateral extent of the charge column. The diameter of this column is determined by the initial ionization along the particle track and lateral diffusion during the collection process. These values are not known accurately, but seem to be of the order of 10 to 100 μm. The resulting series resistance commonly attains values up to 10^3 to 10^4, even in low resistivity ($\rho \sim 10^3$ Ω cm) detectors. The integration time constant $R_S C_i$ resulting from 10 pF input capacitance, for example, is then 10 to 100 ns, typically an order of magnitude greater than the collection time of the detector.

Obviously this series resistance should be eliminated and is one of the main reasons for using totally depleted detectors in timing measurements.

Another reason for avoiding partially depleted detectors stems from the non-uniform dopant concentration in the silicon ingots from which the detector slices are cut. The variation in resistivity can be as high as 20% across the diameter of the detector, leading to a systematic variation in depletion depth with corresponding changes in field strength and collection time over the detector area. The series resistance of the bulk silicon layer also varies accordingly. Measured data on these effects have been published by Henschel, et al.[11] In a totally depleted detector this relative variation in field strength is reduced in proportion to the applied overbias.

The series resistance R_C includes any resistance associated with the detector electrodes and the resistance of connections. Typically, R_C is not more than a few ohms.[14,15] The series inductance L_S is the inductance of the connections. In conjunction with the input capacitance C_i of the preamplifier the series inductance forms a low pass filter, which can severely degrade the signal rise time. The inductance due to a 1 cm length of 0.5 mm diameter wire connecting the detector to a preamplifier with 10 pF input capacitance would by itself result in a rise time of 1 ns. Obviously, detector assemblies using a coiled spring contact should not be used. The series inductance can be reduced by using low inductance capacitors (e.g. monolithic multilayer chip capacitors) and ribbon leads instead of thin wires in the signal path.

The input LC circuit will also tend to 'ring' at its resonant frequency unless it is damped sufficiently by an equivalent series resistance. This can be provided by the real part of the input impedance of the input amplifier, which even for an FET is typically of the order of 10^3 Ω or less at high frequencies. Obviously it would be best to use an input stage presenting an essentially resistive load. This cannot be achieved with conventional FET input stages, but suitable alternatives will be presented in the next section.

The variation of signal propagation time on the electrodes of the detector can also significantly degrade time resolution, especially when large area detectors are used. Sanderson, et. al. have measured a delay of 50 ps for particles impinging at a radius of 4.5 mm with respect to the center of the detector, and a delay of 110 ps at a radius of 7 mm.[12] Increasing the resistive component of the distributed RLC transmission line formed by the electrodes by

making them extremely thin (< 10 μg/cm² Au, for example) will significantly increase the delay and the dispersion, i.e. charges in rise time over the detector area. The variation in delay is especially pronounced when the low resistance connection to the electrode is at only one point, rather than along the whole perimeter of the detector.[13] A 40 μg/cm² circular gold electrode (as commonly used on commercially available detectors) with a low resistance contact made along the entire circumference will exhibit a total resistance of about one ohm and seems to be a reasonable compromise between a minimum dead layer and low resistance. The effect of these changes in delay is reduced for short flight paths between detectors, since the loss of correlation between the positions of incidence on the two detectors due to small angle scattering is reduced. In principle this sytematic deviation could be corrected event by event if the position of incidence were measured.

In the detection of heavy ions the charge collection process is modified by the extremely high density of charge formed along the particle trajectory. The differential energy loss (corresponding to the Bragg peak) is 0.3 MeV/μm for a 0.8 MeV α particle, increasing to 5 MeV/μm for ^{40}Ar at 50 MeV, 10 MeV/μm for ^{84}Kr at 135 MeV and 30 MeV/μm for ^{238}U at 1 GeV particle energy.[16] These values should be compared to 0.4 keV/μm energy loss for 1 MeV electrons, corresponding to an increase by a factor of 10^3 to 10^5 for the heavy ions over minimum ionizing particles. The resulting charge density is so high that the electric field in the detector volume cannot penetrate the plasma column. Therefore, it initially expands by ambipolar diffusion,[17] until the plasma is sufficiently dilute for the electric field to penetrate it and act on the charges. The collection process can be accelerated by a sufficiently large electric field eroding the plasma at the surface, thereby whittling it down.

We should therefore expect the "plasma effect" to manifest itself in two ways: 1) the signal induced on the electrodes will be delayed, since the plasma sheath remains neutral during the initial ambipolar diffusion phase (plasma delay). 2) collection time will increase due to the gradual erosion of the plasma. Since the time required for the plasma to dilute sufficiently for the external field to act on the charges is subject to statistical uncertainties, one should also expect a plasma jitter to be associated with the plasma delay, i.e. a degradation of time resolution. A more detailed discussion of these phenomena has been presented by Tove and Seibt.[18,19]

Despite the large number of papers published on the subject of plasma effects, there is little (if any) reliable data on how they quantitatively affect time resolution. This is due to the fact that very few investigators have adequately determined the characteristics of their timing electronics. Excellent data on plasma delays have been published by Henschel, et al[20,21], indicating a constant value of 3 ns for fission fragments and 1.4 ns for 6.1 MeV α particles at low fields. At field strengths greater than 10^4 V/cm for fission fragements and $3 \cdot 10^3$ V/cm for alpha particles the plasma delay decreases with increasing field strength as E^{-1}.

The particle dependence of the plasma delay alters the mass calibration of a time-of-flight spectrometer. How plasma delay quantitatively affects time resolution is not known. In a recent experiment at the Argonne Superconducting Heavy Ion Linac the author, together with W. Heming, D. Kovar and R. Pardo measured 32 ps time resolution with 230 MeV ^{28}Si ions in a closely spaced pair of detectors. Within the errors of a few percent the measured resolution was determined solely by the timing electronics, indicating an upper limit of 10 ps for plasma jitter. Average field strengths in the 27 μm thick ΔE detector and 142 μm thick E detector were $1.1 \cdot 10^4$ V/cm and $2.0 \cdot 10^4$ V/cm, respectively. The ratio of maximum to minimum field strength was 1.3 in the ΔE and 1.2 in the E detector, ensuring a high field throughout the length of the particle track.

The presence of plasma effects can be estimated by observing the shape and rise time of the detector pulse with increasing detector bias and comparing this with the expected behavior for unretarded charge collection. Measurements of this type indicate that plasma effects are negligible for "light" heavy ions with A < 50 if the field strength E along the particle track is $2 \cdot 10^4$ V/cm or more. E > $3 \cdot 10^4$ V/cm seems to be adequate up to A ≈ 100, whereas field strengths of 5 to $7 \cdot 10^4$ V/cm (or more?) are required for lead and uranium ions. The latter fields are only obtainable with exceptional detectors, however, field strengths of 2 to $3 \cdot 10^4$ V/cm can be readily achieved.

At first glance it would appear that plasma erosion could be accelerated if the electric field were oriented perpendicular to the particle track, not parallel as is usually the case. As pointed out by Tove and Seibt[18] this is irrelevant, since the high conductivity of the plasma column will deform the electric field, so that locally it will automatically be oriented normal to the surface of the plasma.

Plasma erosion can also be accelerated by cooling the detector. At a field strenght of 10^4 V/cm the drift velocity nearly doubles when the detector is cooled from 300 K to 77 K (the relative increase in velocity is significantly greater at low fields).[22] It is doubtful whether this modest increase is really worth the bother of cooling to liquid nitrogen temperature. On the other hand, it does show that there is not much to be gained in this regard by cooling the detector by 20 or 30 degrees, as is often done.

In conclusion it can be said that, despite frequent claims to the contrary, plasma effects are not the main source of timing uncertainty for light- and medium-mass heavy ions - provided the basic rule of having sufficient field strength along the particle track is observed. In the highest resolution heavy ion time-of-flight measurements done today, timing jitter is determined by electronics.

4. AMPLIFIERS

A. General Comments

The first stage of the amplifier must provide the proper load for the detector. It must also exhibit low noise and sufficient gain, so that noise from subsequent stages does not contribute significantly. The rise time of the amplifier should correspond to the maximum rate of change dV/dt of the detector pulse. Increasing the bandwidth of the amplifier increases the noise more than dV/dt. Decreasing the bandwidth decreases dV/dt more rapidly than the noise, which is proportional to the square root of bandwidth. Restricting the low frequency response, i.e. clipping, offers practically no advantage - except in the presence of low frequency noise (e.g. power line noise) - since a significant reduction in

noise bandwidth will tend to roll off the pulse transition, degrading $(dV/dt)_{max}$ more than the noise is reduced.*

B. Voltage vs Current Mode

In principle, it is possible to exploit either the current pulse or the voltage pulse of the detector for timing purposes. The current pulse has the fastest rise time - only dependent on the external circuitry. The short collection times of thin detectors also result in sufficiently large instantaneous currents. The voltage pulse is formed by integrating the current pulse on the detector capacitance. Its rise time is equal to the width of the current pulse and at first glance would seem to be inferior. Why, then, is the voltage mode used almost exclusively?

The criteria for current and voltage mode operation are given in Fig. 8. If the input time constant formed by the detector capacitance and the input resistance of the preamplifier $\tau_i = R_i C_D$ is much smaller than the collection time, the detector capacitance will discharge faster than charge is induced on it by the collection process. The current into the input of the preamplifier is then equal to the signal current due to movement of charge carriers in the detector: current mode. If the input time constant $R_i C_D$ is large compared to the collection time, the induced charge will remain on the detector capacitance and be transformed to a voltage $V = Q/C$: voltage mode.

The collection times in thin detectors are a few nanoseconds or less. The input time constant for current mode operation would therefore have to be of the order of 100 ps. For a 100 pF detector the input resistance must then be one ohm or less in the gigahertz range. Higher capacitance detectors are commonly used and would require even lower values of input resistance. With present day components it is impossible to achieve such low values of input resistance at high frequencies. Therefore, in a system using thin, high capacitance detectors there is, for all practical purposes, no such thing as a current sensitive preamplifier.

The following discussion will therefore be formulated in terms of input voltages. In the voltage mode the detector can be considered as a low impedance voltage source. For a given input equivalent noise voltage, all situations with the same ratio of detected energy to detector capacitance will provide the same signal-to-noise ratio.

C. Noise Sources

In the frequency range of interest here, the dominant noise sources have a uniform spectral density, i.e. they are "white". Furthermore, no complex pulse shaping is involved: the passband of the amplifier is essentially flat with an upper frequency cutoff. Therefore, the noise analysis can easily be performed in the frequency domain.

*This statement is not valid if the pulse transition is determined by only one integration time constant, where dV/dt is maximum at the origin t = 0. In practice the transition is formed by multiple integration, leading to an initial curvature before the region of maximum slope is reached.

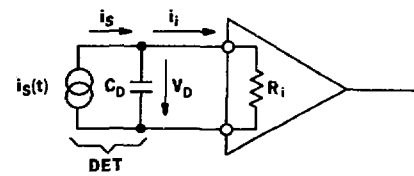

$\tau_i = R_i C_D$

$\tau_i \ll t_{COLL} \rightarrow i_i = i_S$ CURRENT MODE

$\tau_i \gg t_{COLL} \rightarrow i_i \ll i_S$ VOLTAGE MODE

$$V_D = \frac{\int i_S dt}{C_D}$$

$$V_D = \frac{Q}{C_D}$$

XBL 822-8103

Fig. 8. Criteria for current and voltage mode operation.

The combined effect of all input noise sources can be expressed by two parameters: an equivalent input noise voltage e_n and an equivalent input noise current i_n, as shown in Fig. 9. The noise current flows through the source impedance Z_S resulting in a noise voltage $i_n \cdot Z_S$. This adds to the equivalent input noise voltage e_n, resulting in the total equivalent input noise voltage

$$e_{n\,tot} = \sqrt{e_n^2 + (i_n Z_S)^2} \qquad (14)$$

The main reason for using field effect transistors as the input device in semiconductor detector preamplifiers is their extremely low equivalent input noise current - mainly determined by the gate leakage current which is typically six or more orders of magnitude less than the base current in bipolar transistors. The relevant quantity, however, is the product $i_n Z_S$: low capacitance detectors used with microsecond peaking times (corresponding to low frequencies) exhibit a high impedance $Z_S = X_C = 1/\omega C$ and, conversely, high capacitance detectors used with nanosecond peaking times (corresponding to high frequencies) present a low impedance, where the product $i_n \cdot Z_S$ may be negligible compared to the equivalent input noise voltage e_n. The former situation corresponds to a typical high-resolution gamma or x-ray spectrometer, whereas the latter represents a fast timing system as considered here. The noise characteristics of field effect transistors and bipolar transistors will therefore be examined.

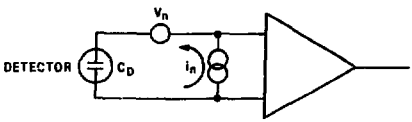

	$v_n\left[\frac{nV}{\sqrt{Hz}}\right]$	$i_n\left[\frac{pA}{\sqrt{Hz}}\right]$
FET	1.6	10^{-2}
BIPOLAR TRANS.	0.4	1

XBL 822-8104

Fig. 9 Equivalent noise voltage e_n and equivalent noise current i_n are generalized parameters which characterize noise performance of an amplifier for any source impedance.

D. Noise in Field Effect Transistors

The dominant noise source in an FET is the thermal noise associated with the channel resistance. The equivalent input noise density (i.e. referred to 1 Hz bandwidth) is[23,24]

$$v_n^2 = 4kT\,R_n \qquad (15)$$

where

$$R_n = \frac{0.7}{g_m}\left(1 + \frac{1}{3}\frac{C_{GS}}{C}\right) \qquad (16)$$

g_m being the transconductance of the FET, C_{GS} the gate source capacitance and C the total input capacitance $C_i + C_D$. R_n is the equivalent noise resistance. The first term in Eq. 16 is the channel noise, the second term represents channel noise fed back to the gate. In the following discussion the equivalent noise resistance will be simplified to

$$R_n = \frac{1}{g_m} \qquad (17)$$

since this does not modify the salient points to be made.

The detector signal is

$$V_s = \frac{Q}{C_i + C_D} \qquad (18)$$

The signal-to-noise ratio is given by

$$\frac{v_s^2}{v_n^2} = \frac{Q^2}{(C_i + C_D)^2} \cdot \frac{g_m}{4kT} \qquad (19)$$

The ratio g_m/C_{GS} is determined by device geometry, specifically by the ratio of gate width to gate length. For a given "generation" of devices g_m/C_{GS} will therefore tend to be constant. If we substitute

$$K = \frac{g_m}{C_{GS}} = \text{const} \qquad (20)$$

in the equation for signal-to-noise ratio (19) we obtain (assuming $C_i = C_{GS}$)

$$\frac{v_s^2}{v_n^2} = \frac{KQ^2}{4kT} \cdot \frac{C_i}{C_i + C_D} \qquad (21)$$

which assumes its maximum value for $C_i = C_D$ reflecting the fact that increasing C_i decreases the signal and the noise in different proportions. It should be emphasized that the matching condition $C_i = C_D$ has no profound significance (such as requiring equal sharing of charge, for example). It is a trivial consequence of the linkage between input capacitance and transconductance in an FET. A transistor which does not fulfill the matching condition may nevertheless be superior to one that does, because of a larger ratio g_m/C_{GS}. High frequency devices tend to have low input capacitance, so that the matching condition cannot be fulfilled for high capacitance dtectors.

An FET with $g_m = 20$ mS should exhibit a spectral noise density of $v_n = 0.8\ nV/\sqrt{Hz}$. Wideband measurements of U310 and SD203 devices yield $v_n \approx 1.6\ nV/\sqrt{Hz}$. This discrepancy between theory and experiment is consistent with other measurements.[25] GaAs FETs have high g_m/C_{GS} ratios and seem promising. Measured noise density is typically 1.0 to 1.3 $nV/\sqrt{Hz}$ in the frequency range 100 to 500 MHz. These devices provide low noise figures in narrow band applications (F ≈ 0.7 dB) by virtue of their high input impedance which allows a significant voltage step up in a 50 Ω system. GaAs FETs also tend to exhibit increasing noise at frequencies below 500 MHz or so. A further disadvantage is their extreme susceptability to gate breakdown.

E. Noise in Bipolar Transistors

The significant high frequency noise sources in a bipolar transistor input stage are shown in Fig. 10.[25,26] R_s is the resistive part of the source impedance Z_s, with its associated noise generator $v_n^2 = 4kTR_s$. The base spreading resistance r_b' also has an associated noise generator $v_n^2 = 4kTr_b'$. The shot noise component of the base current I_b is $i_b^2 = 2e\,I_b$, where e is the electron charge. $Z_{b'e}$ is the internal base emitter impedance. The shot noise associated with the collector current $i_c^2 = 2e\,I_C$ must be transformed to the input to yield the equivalent input noise voltage

$$v_n^2 = 4kT\,(r_b' + R_s') + 2e\,I_b\,(r_b' + Z_s)^2 + 2e\,I_C\left(\frac{Z_s + r_b' + Z_{b'e}}{g_m\,Z_{b'e}}\right)^2 \qquad (22)$$

where the fraction in the last term is the reciprocal effective transconductance g_m^{eff} of the transistor. This term determines the frequency dependence of the transistor noise. As a low frequency approximation, using the relationships $g_m = 1/r_e$ and $I_C = I_E = kT/er_e$ the collector term can be written $2kTr_e$, often called the "noise of the emitter resistance". This is a misnomer, since the dynamic emitter resistance r_e does not produce thermal noise (this fact will be exploited later). This resistance per se is noiseless, the only noise associated with it being due to the current flow

over the potential barrier of the base-emitter diode, i.e. shot noise. Misleading as it may be, the formulation $2kTr_e$ is useful as an estimate of this term in comparison to the first. This last term can also be formulated in terms of the internal base emitter capacitance, since $g_m = C_{b'e} \cdot \omega_T$ in the hybrid π model, where ω_T is the transit frequency. This also yields *a matching condition between input capacitance and* source capacitance, as for the FET.

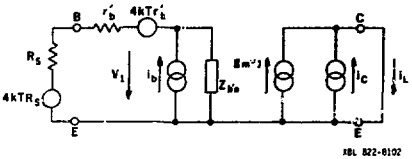

Fig. 10. Noise sources in a bipolar transistor.

The problem in evaluating Eq. 22 is that the parameters r_b' and g_m^{eff} are usually not specified for the transistor of interest. However, g_m^{eff} can readily be calculated from S-parameters, which are usually specified for high frequency devices. The base spreading resistance can be determined from a noise figure measurement. Noise figure F is defined as

$$F = \frac{v_n^2}{4kTR_S}, \qquad (23)$$

often expressed in dB. If the noise figure is known for a given source resistance, Eqs. 23 and 22 may be used to determine the base spreading resistance.*

Applying this method to a type BFT66 transistor (F = 1.26 at 10 MHz and F = 1.4 at 500 MHz) yields $r_b' \approx 6\ \Omega$. For a capacitive source C_D with $R_S \approx 0$ - corresponding to a gr . detector - the terms of Eq. 22 written in the same order are then

$$v_n^2 = 9.6 \cdot 10^{-20} + 4.8 \cdot 10^{-23} \left(6 + \frac{1}{\omega C_D}\right)^2 + 6.4 \cdot 10^{-20}$$

The second term due to the base shot current increases with ω^{-1}, necessitating the introduction of a lower cutoff frequency to optimize noise performance. In a passband of 20-350 MHz (adequate for a rise time of one nanosecond) the noise contribution due to this term is negligible for a detector capacitance $C_D >$ 100 pF. The spectral noise density is then

$$v_n = 0.4\ nV/\sqrt{Hz}$$

dominated by the thermal noise associated with r_b' and the collector shot noise.

Measurements on actual circuits provide the same result, corresponding to an equivalent input noise $v_n = 7.5$ nV at 350 MHz bandwidth, i.e. 1 ns rise time. Comparable results are obtained with the devices BFT97, BFQ69 (Siemens) and NE645 (NEC)**, where the latter two are probably the best devices currently available for this application. Equivalent input noise of 6.5 nV over a 500 MHz bandwidth has been measured on several BFQ69 stages without selecting devices for low noise. General selection criteria when scanning data sheets for suitable transistors are: high gain-bandwidth product ($f_T > 3$ GHz), low noise figure ($F \leq 1$ dB at 500 MHz) and high dc current gain, representing the third, first and second *term in Eq. 22 respectively.*

In summary, the preceding discussion has shown that, contrary to widespread belief, bipolar transistors are superior to field effect transistors (FETs) for fast timing with moderate and high capacitance detectors. This is true for current devices. Improvements in GaAs FETs could shift the balance in their favor. On the other hand, improvements in *bipolar transistors are equally probable. Currently,* performance, ease of application and price certainly favor bipolar transistors.

Now that amplifier noise levels have been determined, we can estimate the importance of detector noise. The noise sources associated with the detector are series resistance, which we will assume to be small with respect to r_b', and shot noise $i_n^2 = 2eI_r$ associated with the reverse junction current I_r. This has the same effect as the base current shot noise in a bipolar transistor and is negligible for reverse junction currents up to several microamperes in a 100 pF detector. Detector noise, therefore, is not a practical problem in these applications, since moderate cooling will reduce leakage current to acceptable levels, if necessary.

F. Coupling the Detector to the Preamplifier

Four methods of deriving both a timing and an energy signal from a semiconductor detector are shown in Fig. 11. A charge sensitive preamplifier is well suited for timing with thick, low capacitance detectors, where collection times are long (Fig. 11a). If the collection time exceeds the rise time of the preamplifier there is no point in using a more complex system: this is the optimum - and most convenient - configuration. Response time of a fast (stable) charge sensitive preamplifier for low capacitance detectors is about 5 ns, increasing with detector capacitance. Thin detectors with short collection times and high capacitance require a hybrid approach.

Figure 11b uses a current sensitive preamplifier in series with the detector. Since the charge sensitive preamplifier does not exhibit a low impedance at high frequencies, a capacitor parallel to its input is required to provide a fast signal return path. As was explained in the discussion of current vs. voltage mode this is usually not a practical configuration.

Figure 11c shows a high impedance voltage sensitive preamplifier connected parallel to a charge sensitive preamplifier. This is feasible because of the limited response speed of the charge sensitive loop. Charge is first integrated on the detector capacitance and the resulting voltage pulse sensed by the fast voltage sensitive preamplifier. As the charge sensitive loop becomes active, charge is transferred from the detector electrodes to the preamplifier's large dynamic input capacitance. The response time of the charge sensitive amplifier therefore determines the

*This is probably the most accurate (or least inaccurate) method of determining r_b' (Ref. 27).

**Reference to a company or product name does not imply approval or recommendation of the product by the University of California or the U.S. Department of Energy to the exclusion of others that may be suitable.

decay time of the voltage pulse. The input resistance of the voltage preamplifier must be very large so that it does not prematurely discharge the detector capacitance before the charge loop is active. For all practical purposes this requirement dictates use of an FET input stage. A resistor in series to the input of the charge sensitive amplifier isolates its quiescent input capacitance from the fast channel. The thermal noise of this resistor can be short circuited at low frequencies by a shunt inductor (not shown) to reduce its contribution to the charge sensitive channel. The values of the resistor and inductor are not critical, although the inductor must have low resistance. A voltage sensitive system which has found widespread use was published by Sherman, et al.[28]

A transformer coupled system is shown in Fig. 11d. This can be either current or voltage sensitive. In its originally published form[29] this circuit was used to sense the current flowing into a charge sensitive preamplifier, obviously limiting its effectiveness. A voltage sensitive scheme will be presented later.

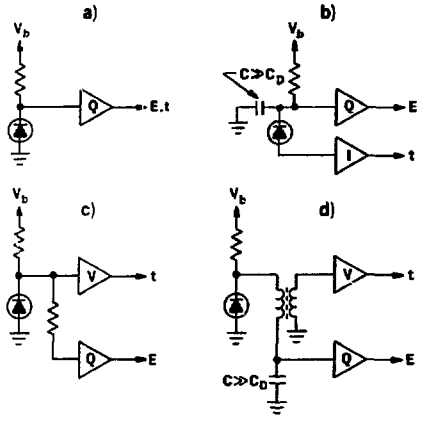

Fig. 11. Methods of deriving an energy and a timing signal from a detector.

The fast-slow preamplifier concept combines a charge and a voltage sensitive amplifier in one circuit.[30,31] The fast signal is taken off at an early stage of a charge sensitive preamplifier circuit where bandwidth is still large. The voltage signal builds up in the open loop mode of amplifier operation and decays with the response time of the charge loop. This scheme is elegant and convenient to use. However, since the input stage must work well at both low and high frequencies, it does require some design compromises not necessary in the hybrid scheme. It is often overlooked that this configuration requires a dual noise specification: equivalent noise charge for the slow channel and equivalent input noise voltage for the fast channel.

G. Resistively Terminated Systems

One widespread misconception is that it is necessary to mount the input stage of the preamplifier in immediate proximity of the detector ("head mounted" preamplifier). Consider a transmission line connected to the detector and terminated at its far end with a resistance equal to the line's surge impedance Z_0. The transmission line will then present a purely resistive load Z_0 to the detector. If the condition $\tau_i = Z_0 \cdot C_D \gg t_{coll}$ for voltage mode operation is fulfilled (Fig. 8) there will be no significant loss in signal level due to the decay of the signal. Signal degradation, even in thin (~ 3 mm diameter) coaxial cables, is no problem: the rise time of a one meter length of cable is a few hundred picoseconds, signal attenuation is not more than a few percent. One argument often brought up against this scheme is that "cables are noisy". This is a myth: the noise of the cable can hardly be measured. Cables can introduce ground loops, and pickup of external signals can be significant if shield coverage is poor and connectors are poorly mounted (check your cables!, but these problems can be avoided. The advantage of this arrangement is that preamplifiers do not have to be mounted in vacuum and can also be replaced quickly during an experiment. One preamplifier can also be easily used with different detectors. Of course, the input condition $\tau_i \gg t_{coll}$ must be fulfilled: a 200 pF detector and 200 Ω line impedance yield $\tau_i = 10$ ns, which is sufficient for a 1 ns rise time.

Two methods of obtaining a resistive input impedance in a hybrid voltage sensitive system without a significant noise penalty are shown in Fig. 12. In Fig. 12a the series resistance used to isolate the fast input from the charge sensitive preamplifier (cf. Fig. 1c) is equal to the line impedance. Its ground return is provided by a capacitor at the charge sensitive amplifier port, resulting in a high frequency termination. A value of 500 to 1000 pF for this capacitor results in a good match over an adequate frequency range. This capacitor does increase the noise in the charge sensitive channel, which is tolerable in this application since the energy resolution for heavy ions will still be limited by processes in the detector.[32,33] Low frequency thermal noise due to the termination resistor is short circuited by the shunt inductor (L = 10 to 20 μH). The resistive termination does increase noise in the fast channel. However, its equivalent noise resistance is decreased by a factor $[X_C/(X_C + R_T)]^2$, where X_C is the reactance of the detector and R_T the termination resistance. In most cases the noise contribution due to the termination is therefore negligible compared to the noise of the input FET. The fast amplifier must have a low input capacitance to avoid significant degradation of rise time and impedance matching (10 pF ≙ 45 Ω at 350 MHz).

This simple scheme is not amenable to bipolar input stages. Furthermore, in many situations the shunt resistor would significantly degrade the extremely good noise performance offered by bipolar transistors. The voltage sensitive transformer coupled circuit shown in Fig. 12b is free of these limitations. A

fast preamplifier providing a wideband fixed termination is coupled to the detector through a transformer. The transformer is designed for a lower cutoff frequency high enough to avoid appreciable coupling of noise from the fast to the slow channel. This being a matched system (contrary to transformer coupled circuits published heretofore), a transmission line transformer with excellent high frequency characteristics (f_{max} = 1 GHz) can be used.[34] The current flowing from the detector through the transformer primary is integrated on the capacitor C. This charge is subsequently transferred to the charge sensitive preamplifier. The remaining problem is how to design a low-noise fast amplifier with a well defined resistive input impedance.

TERMINATED SYSTEMS

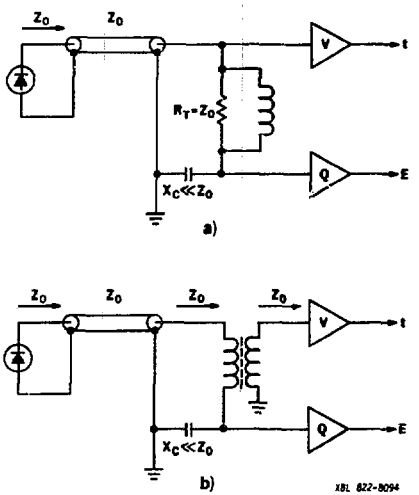

Fig. 12 Terminated systems using a cable between detector and preamplifier.

H. *Cooled Terminations in Subnanosecond Amplifiers*

The concept of "cooled terminations", i.e. essentially noiseless resistive loads corresponding to low noise temperature, has been applied by Radeka[35] to circuits where a 90° phase shift in the forward path of a feedback loop transforms a feedback reactance to a resistance at the amplifier input. However, ensuring a 90° phase shift up to subnanosecond bandwidths is practically impossible. Other schemes have to be applied here.

A circuit using a transformer as the feedback element is shown in Fig. 13. Published (and patented) by Norton,[36] this circuit ideally has neither losses nor thermal noise associated with the feedback element, hence the term "lossless" or "noiseless" feedback.[36,37] Obviously, the characteristics of the transformer are crucial: its geometry must provide low interwinding capacitance and a small leakage inductance for good high frequency performance. Core losses must be low since any resistive component will introduce additional noise. This is especially important at high frequencies which determine the noise bandwidth. The windings must also exhibit enough self inductance for adequate low frequency response. A passband of 10 to 400 MHz has been obtained with a voltage gain of three in a 50 Ω circuit. The input reflection coefficient is less than 15% throughout the passband. The circuit will handle input levels up to several hundred millivolts. Noise performance equals that of the transistor without feedback.

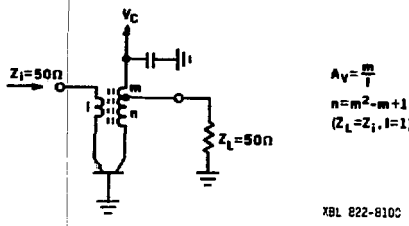

Fig. 13. A circuit using a transformer as a "noiseless" feedback element.

A simpler circuit is shown in Fig. 14. Figure 14a shows a conventional series shunt feedback stage with simplified design equations.[38] Shunt feedback due to R_F decreases the input impedance, whereas series feedback introduced by R_E increases it. The efficacy of both mechanisms decreases at high frequencies due to decreased transistor gain, but the cumulative effect keeps the input impedance constant. Rigorous calculations using actual transistor parameters (S-parameters) show that the simplified design equations shown in Fig. 14a yield the correct values of R_F and R_E but overestimate the gain by about 10%. Thermal noise due to R_F is significantly attenuated by the source impedance, so that the major source of additional noise is the emitter resistor R_E. This noise source is eliminated by using the dynamic emitter resistance $r_e = kT/eI_E$, i.e. a noiseless resistance, as the series feedback element R_E.

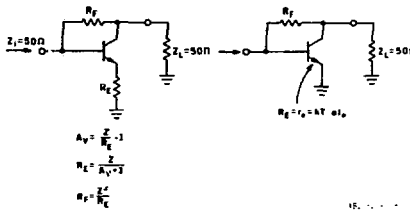

Fig. 14 The series shunt feedback stage (a) where the emitter resistor has been replaced by a "noiseless resistance" (b).

Two cascaded stages of this type using BFQ69 transistors with a total voltage gain of 30 exhibit a rise time of less than 1 ns and an equivalent input noise of 6.5 μV. The input reflection coefficient is < 10 throughout the passband and can be minimized by adjusting the emitter current of the transistor. The drawback of this circuit is its limited dynamic range, since the dynamic emitter resistance is current dependent. However, compromise settings are quite adequate for many applications. The freedom of design and utter simplicity afforded by this circuit make it very convenient to design and construct. It can also be applied to delay line readout of position sensitive detectors, for example.

1. Mismatched Systems

Before concluding this discussion on using transmission lines to connect the preamplifier to the detector, we should consider an imperfect, albeit common situation: a high-impedance amplifier connected through a low-impedance (50 to 100 Ω) cable. How does this mismatched system behave?

A short cable, whose propagation time is small compared to the rise time of the detector pulse, will act as an additional shunt capacitance. This will be smaller for higher impedance cables.

If the cable is long, with a transit time T which is large compared to the rise time, it will initially present a resistance to the detector which is equal to the surge impedance of the cable. This load will only change after a time 2T when the signal reflected from the preamplifier arrives at the detector. At the preamplifier input, the pulse amplitude will increase, since it is refected with equal polarity. However, its rise time will be degraded by the input capacitance. The signal will be reflected back and forth, and finally it will be indiscernable. The dead time of the trigger has to be increased to prevent it from firing consecutively on the reflected pulses. This "sloppy" system is not optimum, the pulses look terrible, but it is usable – although certainly not recommended.

5. THE TRIGGER

The purpose of the trigger is to provide a normalized logic pulse with a well defined time relationship to the time origin of the analog input pulse for all variations of amplitude or shape. The simplest circuit of this kind is a leading edge trigger, which provides a logic output when the input signal exceeds a fixed reference level. As shown in Fig. 15, amplitude variations lead to a shift in timing called "walk". Walk can be reduced by setting the trigger threshold low, but this is in conflict with the requirement that the trigger threshold be set at the point of maximum slope for optimum timing. Another source of walk are variations in rise time.

Amplitude walk can be eliminated by having the trigger threshold track the pulse amplitude (Fig. 16). This is done by delaying the transition of the pulse and comparing it with a fraction f of the pulse amplitude applied to the reference input. The circuit will now trigger at a constant fraction f of pulse amplitude, hence the name constant fraction trigger.[39,40] Amplitude compensation will occur if the delay time t_d is set 20 to 30% larger than the rise time t_r of the input pulse. If the delay is chosen so that

$$t_d < (1 - f)\, t_r$$

The reference level will be a function of both amplitude and rise time. For longer rise times the trigger fraction will shift to smaller values and conversely, shorter rise times will increase the trigger fraction. This mode results in amplitude and rise time compensation, provided that all occurring trigger fractions lie in the linear portion of the pulse transitions.

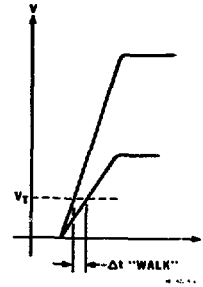

Fig. 15. Amplitude walk in a leading edge trigger.

CONSTANT FRACTION TIMING

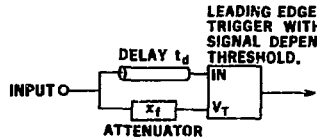

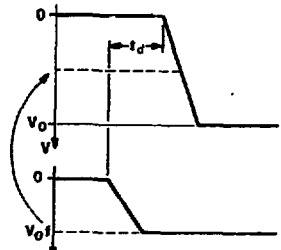

1. $t_d \geq t_r$: $V_T = f \cdot V_O$ ⟶ AMPLITUDE COMPENSATION
2. $t_d < (1-f)t_r$: $V_T = V_T(V_O, t_r)$ ⟶ AMPLITUDE + RISE TIME COMPENSATION

XBL 822-8092

Fig. 16. Principle of constant fraction timing.

Amplitude walk in a good constant fraction trigger is ± 50 ps over a dynamic range of 100:1, exceptional units achieve ± 20 ps. Concentration on reducing the walk of trigger circuits has diverted attention from two important characteristics of a trigger which significantly affect the time resolution of a fast timing system.

The upper curve in Fig. 17 shows the measured time resolution of a better than average leading edge trigger as a function of amplitude for a fixed rise time and noise level. The trigger threshold has been readjusted for each signal level to a trigger fraction of 50% (dV/dt = max). The straight line below the curve indicates the time resolution given by the first term of Eq. 3. For small signal levels the measured curve is nearly parallel to the calculated line. The difference is due to the limited bandwidth of the trigger. At high levels the measured resolution no longer improves with increasing signal-to-noise ratio: it flattens off due to the residual jitter of the trigger circuitry – the second term in Eq. 3. These data were measured on a fast comparator IC – basically a cascade of differential amplifiers. Similar results are also obtained for tunnel diode discriminators.

The data in Fig. 17 correspond to an effective rise time of *about 2 ns. Triggers commonly in use* have effective rise times as long as 5 to 7 ns, the *residual jitter may be as high as to 50 ps, imposing* a severe limit on achievable time resolution.

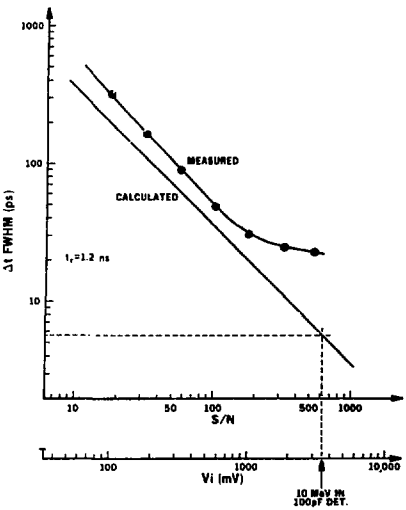

Fig. 17. Resolution vs. externally defined signal-to-noise ratio of a leading edge trigger, where a trigger fraction of 0.5 has been set for every input level v_i.

The trigger also has an effective input noise. This may be determined by measuring the resolution vs. signal level for an essentially noise free input pulse with a rise time which is long compared to the inherent rise time of the trigger. The measurement indicated by the upper curve in Fig. 18 (t_r = 10 ns) *yields an equivalent input noise of about 80 μV rms*, a value typical for fast comparators and ECL circuits. Data published by Leskovar and Lo[41] for a tunnel diode constant fraction trigger indicate an equivalent input noise in excess of 500 μV. This quantity must be known in order to estimate how much insertion gain is required for preamplifier noise to override the equivalent input noise of the trigger, so that system resolution is determined by front end noise.

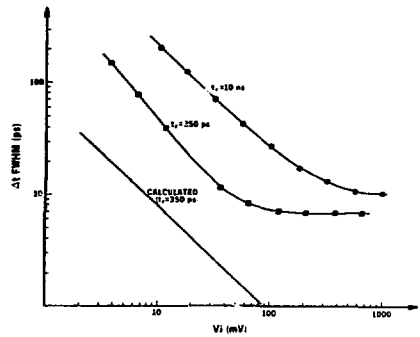

Fig. 18. Measurements to determine the equivalent input noise of a trigger (curve labeled t_r = 10 ns) and its internal rise time (curve labeled t_r = 350 ps). The straight line shows the expected time resolution for the measured equivalent input noise and a rise time of 350 ps.

The pulse used to take the center curve in Fig. 18 had a rise time of 350 ps and a flat top of 10 ns duration. In conjunction with the measured equivalent input noise this measurement also yields the effective bandwidth by comparison with the calculated resolution indicated by the straight line. The residual jitter in these measurements is dominated by the resolution of the time converter (6 ps in the fast rise time measurement). This was degraded further in the measurement with t_r = 10 ns by the larger rise time of the logic pulse applied to the reference input of the TAC. This prototype trigger has significantly less residual jitter than the unit used for the measurement in Fig. 17

A constant fraction trigger can also be viewed (and designed) as a shaper with a subsequent zero crossing trigger (Fig. 19). Timing accuracy is determined by the slope at the crossover point and by the internal noise and residual jitter of the zero-crossing trigger, analogous to the preceeding discussion. Inadequate bandwidth will severely reduce the amplitude of the leading lobe and the slope dV/dt at the crossover point. The width of this lobe is equal to the delay time t_d, which is maximum for amplitude compensation alone. Therefore the delay should not be set up for rise time compensation if this isn't necessary.

ANOTHER VIEW OF CONSTANT FRACTION TRIGGERING:

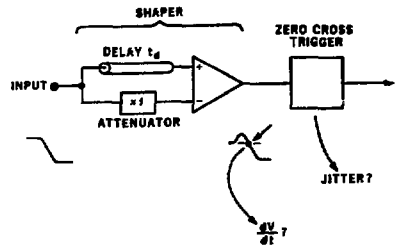

Fig. 19. A constant fraction trigger consisting of a shaper and a zero-crossing trigger.

6. TIME DIGITIZERS

The resolution of time digitizers is usually taken for granted, but at this point it should come as no surprise that it shouldn't be. Figure 20 shows a test setup for measuring the intinsic resolution of a TAC or TDC with random rates. If the fan-out has no time jitter between its two outputs (for example by feeding them from the same current source) the time difference between the start and stop inputs is precisely defined. Any spreading of the time spectrum is then due to the inherent resolution of the time converter.

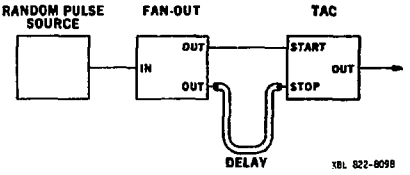

Fig. 20. Configuration used to measure resolution of time converters as a function of random counting rate.

Results on two representative commercial time-to-amplitude converters for random start/stop rates are shown in Fig. 21. Brand O - a unit used in many laboratories - shows significant deviations from a guassian line shape and broadens appreciably when the start/stop rate is increased to 20,000 s-1. Brand C - a new design - has a clean line shape, but also develops a spurious peak which becomes more pronounced with increasing counting rate. These effects disappear when a periodic start/stop rate is applied.

Problems of this sort associated with random rates are not restricted to certain models but plague TACs in general. A notable exception is a rather old design by D. Landis.[42] Linearity should also be checked, specifically in the lowest time ranges which frequently are only partially usable. Improved TACs should be on the market soon.

COUNTING RATE PERFORMANCE OF TAC'S

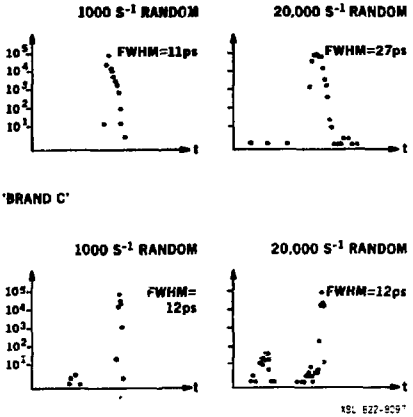

Fig. 21. Resolution and line shape of two time converters at random counting rates (1000 s^{-1} and 20,000 s^{-1}).

7. ANALYZING A SYSTEM

How can the causes of timing uncertainty in a practical experiment be determined? The first step is to measure the contribution due to the electronic part of the system. This can be done by feeding the output of a pulser into the preamplifier input, taking great care that the conditions of the experiment are reproduced. Specifically, this means that the amplitude, rise time and shape of the test pulse must be adjusted to produce the same signal at the input of the trigger as in the actual experiment. The pulser must have a trigger output free of time jitter with respect to the test signal, to provide a reference signal for the time converter. The time resolution is then measured for various pulse amplitudes. The curve in Fig. 17 is the result of such a measurement. If fluctuations in pulse shape were observed, the measurement should be repeated for the range of pulse shapes encountered in the experiment. These data should be taken on every detector channel, even if they seem identical (they often are not, this is the way to find out). On a time-of-flight telescope, the measurement should be repeated with the pulser feeding the start and stop channels. The input signals to the two channels must be independently adjusted to provide the proper amplitude ratios corresponding to the energy deposited in the two detectors.

Feeding the pulser output into the preamplifier is easier said than done, since this should be implemented in a manner that does not change the noise of the system. Using a small test capacitor as is customary in charge sensitive preamplifiers does not work as well with resistive inputs since these two components form a CR differentiation network. The most practical alternative is to disconnect the detector and feed the pulse through a voltage divider providing a very low source resistance (~ 1 Ω), which in turn is connected to the preamplifier input through a capacitor equal in value to the detector capacitance (Fig. 22). This network will closely approximate the source impedance of the detector and also result in the same input time constant. The series resistor in the voltage divider must exhibit low capacitance (< 0.1 pF) whereas the shunt resistor must have a very low stray inductance (< 0.01 nH) to provide a clean pulse at fast rise times.

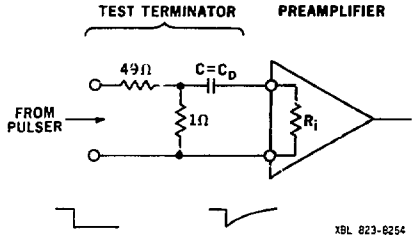

Fig. 22 A test terminator for the measurement of a timing channel's electronic resolution.

A simpler, although less desirable scheme is to feed the preamplifier input directly from a conventional 50 Ω attenuator. This will alter the noise and may change the noise spectrum (if the contribution due to input noise current is significant). In this case the input noise must be measured with the detector and with the attenuator connected to the preamplifier, and the pulser amplitude must be changed accordingly to provide the same signal-to-noise ratio as in the experiment. Measuring the input noise with the detector and with the test fixture connected is advisable in any case.

Noise measurements done by determining the peak noise amplitude on an oscilloscope are at best estimates (usually just "guesstimates": is this equal to 2σ or 3σ?). A true rms noise measurement can be made over a large bandwidth using a diode rectifier in its square law region. At voltages up to about 30 mV the signal current through a semiconductor diode rectifier increases with the square of the input voltage. The rectifier will therefore provide the proper weighting of amplitude fluctuations for a true rms measurement. This result is not affected by any circuitry used to linearize the meter scale. RF millivoltmeters suitable for accurate noise measurements are available with a bandwidth of 1.2 GHz (e.g., Boonton 92B).

The measured noise σ_n and the signal's rate of change at the trigger point $(dV/dt)_{V_T}$ can be inserted in Eq. 2 to determine how good the time resolution should be. The measured resolution indicates how much the electronics should be improved. If the electronic resolution constitutes a significant contribution to the time resolution measured with particles in a detector, improvements in the electronics will result in better time resolution in the experiment. Techniques to evaluate the contributions of the individual electronic modules have been outlined in the preceding sections.

In a system limited by electronic resolution, the measured curve of time resolution vs. input signal can be used to predict experimental results for other energies and detectors (provided the collection times are comparable). The signal levels at the detector can be calculated easily using the numerical equations compiled in the Appendix.

Degradation of resolution not attributable to electronics originates either in the detector or in the geometry of the measurement setup. Variations in length of the flight path are one example of the latter. This could be reduced or eliminated by collimation. In a semiconductor ΔE-E-TOF telescope energy loss straggling in the ΔE detector will lead to variations in flight time. Gating the time spectrum with a window on the energy spectrum, set smaller than the intrinsic resolution of the E detector, will reduce this effect.

And of course there remain the numerous degrading effects in the detector. But the essential point of this discussion is: unless the electronic contributions are carefully and properly measured, any statements regarding the detector's contribution to time resolution are just speculation.

8. FUTURE DEVELOPMENTS

A dashed line in Fig. 17 indicates the time resolution which should be obtainable with 10 MeV energy loss in a 100 pF detector - one with a thickness of 100 μm and an area of 100 mm², for example - given the noise levels in current state of the art preamplifiers. No experiment heretofore has come close to obtaining the predicted value of 6 ps FWHM. Resolution today - at least for light and medium mass heavy ions - is limited by electronics, specifically by bandwidth limitations and residual jitter in the trigger. In most experiments the signal-to-noise ratio is so high that residual jitter is the limiting parameter. The prototype triger whose data is shown in Fig. 18 is already a great improvement in this respect. It may well be that effects in the detector are significant in the region below 10 ps. But, until sufficiently good electronics are available, we really do not know.

9. ACKNOWLEDGMENTS

Preparation of this paper was greatly facilitated by the hospitality extended to me by the Department of Instrument Science and Engineering of the Lawrence Berkeley Laboratory. Skeptical questions from Fred Goulding, Don Landis and Norm Madden provided considerable impetus for me to sort out and clarify my thoughts. This work has certainly benefitted from countless discussions with Michael Maier over the past decade. I also wish to acknowledge Blair Jarrett's assistance in the design of improved triggers.

This work was supported by the Director's Office of Energy Research, Office of High Energy and Nuclear Physics, Division of Nuclear Physics, and by Nuclear Sciences of the Basic Energy Program of the U. S. Department of Energy under Contract DE-AC03-76SF00098.

10. APPENDIX

The following numerical equations are generally useful when working with silicon detectors. The parameters are expressed in units which are commonly used in this application.

d: Depletion depth in μm

V_b: Bias voltage in V

ρ: Resistivity of the semiconductor material in Ω · cm

C_D: Detector capacitance in pF

A: Area of the detector in mm^2

1. Depletion depth of a partially depleted detector:

$$d = \frac{1}{2}\sqrt{\rho \cdot V_b}$$

2. Bias voltage required for total depletion:

$$V_b^D = \frac{4\,D^2}{\rho}$$

where D is the thickness of the detector wafer in μm.

3. Detector capacitance:

$$C_D = \frac{106}{d} \cdot A$$

4. Peak amplitude of the voltage pulse in mV

$$V_S = \frac{44}{C_D} \cdot E$$

where E is the particle energy in MeV.

11. REFERENCES

1. H. Spieler, H.J. Koerner, K.E. Rehm, M. Richter and H.P. Rother, Z. Physik A278, 241 (1976).

2. P.K. Den Hartog, J.L. Yntema, G.E. Thomas and W. Henning, in Preparation of Nuclear Targets for Particle Accelerators, Ed. J. Jaklovsky, Plenum Publ. Corp. p. 29 (1981).

3. N.E. Sanderson, B.R. Fulton and J.B.A. England, Nucl. Instr. and Methods 137, 399 (1976).

4. R. Zierl, H. Essel, P. Kienle, H.J. Koerner, K.E. Rehm, P. Sperr and W. Wagner, Z.Physik A291, 91 (1979).

5. ATLAS: A Proposal for a Precision Heavy Ion Accelerator, Argonne National Laboratory, February 1978.

6. R. Zierl, W. Czech, P. Kienle, H.J. Koerner, K.E. Rehm, P. Sperr and W. Wagner, Nucl. Instr. and Methods 164, 219 (1979).

7. B. Kolb, C. Hlawatsch, G. Rosner, T. Walcher, H. Ingwersen, E. Jaeschke and R. Repnow, Nucl. Instr. and Methods 188, 555 (1981).

8. A.C. Prior, J. Phys. Chem. Solids 12, 175 (1959).

9. S. Ramo, Proc. IRE 27, 584 (1939).

10. G. Cavalleri, G. Fabri, E. Gatti and V. Svelto, Nucl. Instr. and Methods 21, 177 (1963) and Nucl. Instr. and Methods 92, 137 (1971).

11. K. Henschel, H. Hipp, A. Kohnle and F. Goennenwein Nucl. Instr. and Methods 125, 365 (1975).

12. N.E. Sanderson, J.B.A. England, E.C. Pollaco and R.K. Bhowmik, Nucl. Instr. and Methods 153, 93 (1978).

13. F.S. Goulding and D.A. Landis, private communication.

14. G. Fabri and V. Svelto, Nucl. Instr. and Methods 35, 83 (1965).

15. H. Spieler, Ph.D. Thesis, Tech. Univ. Muenchen, 1974 (unpublished).

16. L.C. Northcliffe and R.F. Schilling, Nuclear Data Tables, A7, No. 3 and 4, 233 (1970).

17. G. Dearnaley and D.C. Northrop, Semiconductor Detectors for Nuclear Radiations, John Wiley, Inc., New York, pp. 67-68 (1963).

18. P.A. Tove and W. Seibt, Nucl. Instr. and Methods 51, 261 (1967).

19. W. Seibt, K.E. Sundstrom and P.A. Tove, Nucl. Instr. and Methods 113, 317 (1973).

20. H.O. Neidel and H.Henschel, Nucl. Instr. and Methods 178, 137 (1980).

21. H. Henschel and R. Schmidt, Nucl. Instr. and Methods 151, 529 (1978).

22. A. Alberigi Quaranta, M. Martini, G. Ottaviani, G. Redaelli and G. Zanarini, Solid State Elec. 11, 685 (1968). Data also in G. Bertolini, A. Coche (Ed.), Semiconductor Detectors, North Holland Publ. Co., Amsterdam, p. 69 (1968).

23. a) A. van der Ziel, Proc. IRE 50, 1808 (1962):

b) Proc. IRE 51, 461 (1963):

c) W.C. Bruncke and A. van der Ziel, IEEE Trans. Elec. Devices ED-13, 323 (1966).

24. V. Radeka, IEEE Trans. Nucl. Sci. NS-11/3, 358 (1964).

25. C.D. Motchenbacher and F.C. Fitchen, Low Noise Electronic Design, John Wiley and Sons, New York (1973).

26. A. van der Ziel, Proc. IRE, 1019 (1958).

27. H.F. Cooke, Proc. IEEE 59/8, 1163 (1971).

28. I.S. Sherman, R.G. Roddick, R.J. Metz, IEEE Trans. Nucl. Sci. NS-15/3, 500 (1968).

29. C.W. Williams and J.A. Biggerstaff, Nucl. Instr. and Methods 25, 370 (1964).

30. F. Gabriel, H. Koepernik and K. Schops, Nucl. Instr. and Methods 103, 501 (1972).

31. Y.U. Akimov, K. Andert, A.I. Kalinin and H.G. Ortlepp, IEEE Trans. Nucl. Sci NS-19/3, 404 (1972), and Nucl. Instr. and Methods 104, 104 (1972).

32. F.S. Goulding and B.G. Harvey, Ann. Rev. Nucl. Sci. 25, 167 (1975).

33. J. Lindhard and V. Nielsen, Phys. Lett. 2, 209 (1962).

34. C.L. Ruthroff, Proc. IRE 47, 1337 (1959).

35. V. Radeka, IEEE Trans. Nucl. Sci. NS-21, 51 (1974).

36. D.E. Norton, Microwave Journal, p. 53, May (1976).

37. U.L. Rohde, 1979 IEEE National Telecommunications Conference Record NTC 79 22.6/1-6.

38. R.G. Meyer, R. Eschenbach and R. Chin, IEEE J. Solid State Circuits SC-9, 167 (1979).

39. R.L. Chase, Rev. Sci. Instr. 39, 1318 (1968).

40. M.R. Maier and P. Sperr, Nucl. Instr. and Methods 87, 13 (1970).

41. B. Leskovar and C.C. Lo, Nucl. Instr. and Methods 123, 145 (1975).

42. D.A. Landis, Lawrence Berkeley Laboratory, Time-to-Amplitude Converter, LBL documentation number 11X558.